PERGAMON

Journal of Structural Geology 25 (2003) 1917–1931

JOURNAL OF STRUCTURAL GEOLOGY

www.elsevier.com/locate/jsg

Slip vectors of the surface rupture of the 1999 Chi-Chi earthquake, western Taiwan

Yuan-Hsi Lee[a,*], Meng-Long Hsieh[b], Shih-Ding Lu[a], Tung-Sheng Shih[a], Wei-Yu Wu[a], Yuichi Sugiyama[c], Takashi Azuma[d], Yoshihiko Kariya[e]

[a]*Central Geological Survey, ROC, PO Box 968, Taipei, Taiwan, ROC*
[b]*Department of Geosciences, National Taiwan University, No. 1, Sec. 4, Roosevelt Rd., Taipei, Taiwan, ROC*
[c]*Geological Survey of Japan, 1-1 Higashi, Tskuba, Ibaraki 3058567, Japan*
[d]*Prime Minister's Office, 3-8-1 Ka-sumigashki, Chiyoda-ku, Tokyo 100-0031, Japan*
[e]*Graduate School of Science and Technology, Chiba University, 1-33 Yayoi, Inage-Ku, Chiba 263-8522, Japan*

Received 7 July 2001; received in revised form 28 January 2003; accepted 6 February 2003

Abstract

About 100 slip vectors were surveyed along the 1999 Chi-Chi earthquake rupture (100 km long), western Taiwan, to understand the coseismic reverse-faulting processes. The surveyed slip azimuths vary locally (over 80°) where the rupture is irregular or associated with flexure. Even where the rupture is straight and has consistent slip azimuths, the fault-scarp heights, horizontal slips and fault dip-angles oscillate in a distance of hundreds of meters along the rupture. Despite these local variations, the net slip (up to 11.5 m), vertical and horizontal slips are significant greater in the north, on which maximum shortening (6 m; by pure thrust) and strike slip (8 m; by left-lateral fault) occur in association with the bend of the rupture. The slip azimuths also progressively rotate from north/northwest in the north to west/southwest in the south. These patterns generally agree with those revealed by GPS surveys, except that the slips by GPS in the south move to the west/northwest and have values unexpectedly smaller than our measurements. Our obtained SW-directed slips resulted in dominantly right-lateral faulting (up to 2.4 m) where the rupture ends to the southeast. This, however, does not correspond to focal mechanisms of any main shocks or aftershocks.

Keywords: Slip vector; Surface rupture; Chi-Chi earthquake; Thrust fault

1. Introduction

The September 21, 1999 Chi-Chi earthquake ($M_w = 7.6$), a consequence of on-going collision between the Philippine Sea plate and Eurasian plate (Fig. 1), produced a surface rupture about 100 km long in western Taiwan. The rupture has a throw of up to 10 m, one of the largest coseismic displacements ever documented on a reverse fault. Most of the rupture traversed urban areas and farmed fields, and consequently offset many artificial structures such as city streets, water pipes and fences. These deformed structures record the characteristics of the faulting (e.g. Sharp, 1975) and provide a rare opportunity to examine near-surface reverse-faulting processes during a great earthquake. In this paper, we present surveyed slip vectors and their associated faulting parameters such as shortening, strike-slip components and fault-dip angles, for 98 sites on this rupture.

Our obtained slip vectors and faulting parameters show significant local variations, along with changes in orientation and/or geometry of the rupture. These variations highlight the complexity of the rupturing processes near the surface, a feature perhaps common on reverse faults. Still, our data show distinct regional patterns. We believe that with the number and the quality of the data, these patterns are of significance and should reflect the properties of the fault in the deeper crust. These data are then compared with known earthquake source parameters derived from seismological records (Kao and Chen, 2000; Mori and Ma, 2000; Ma et al., 2001) and with the syn-earthquake rock movement data from GPS surveys (Yu et al., 2001).

* Corresponding author. Tel.: +886-2-2946-2793 ext.245; fax: +886-2-2942-9291.
E-mail address: dljp@linx.moeacgs.gov.tw (Y.H. Lee).

0191-8141/03/$ - see front matter © 2003 Elsevier Ltd. All rights reserved.
doi:10.1016/S0191-8141(03)00039-7

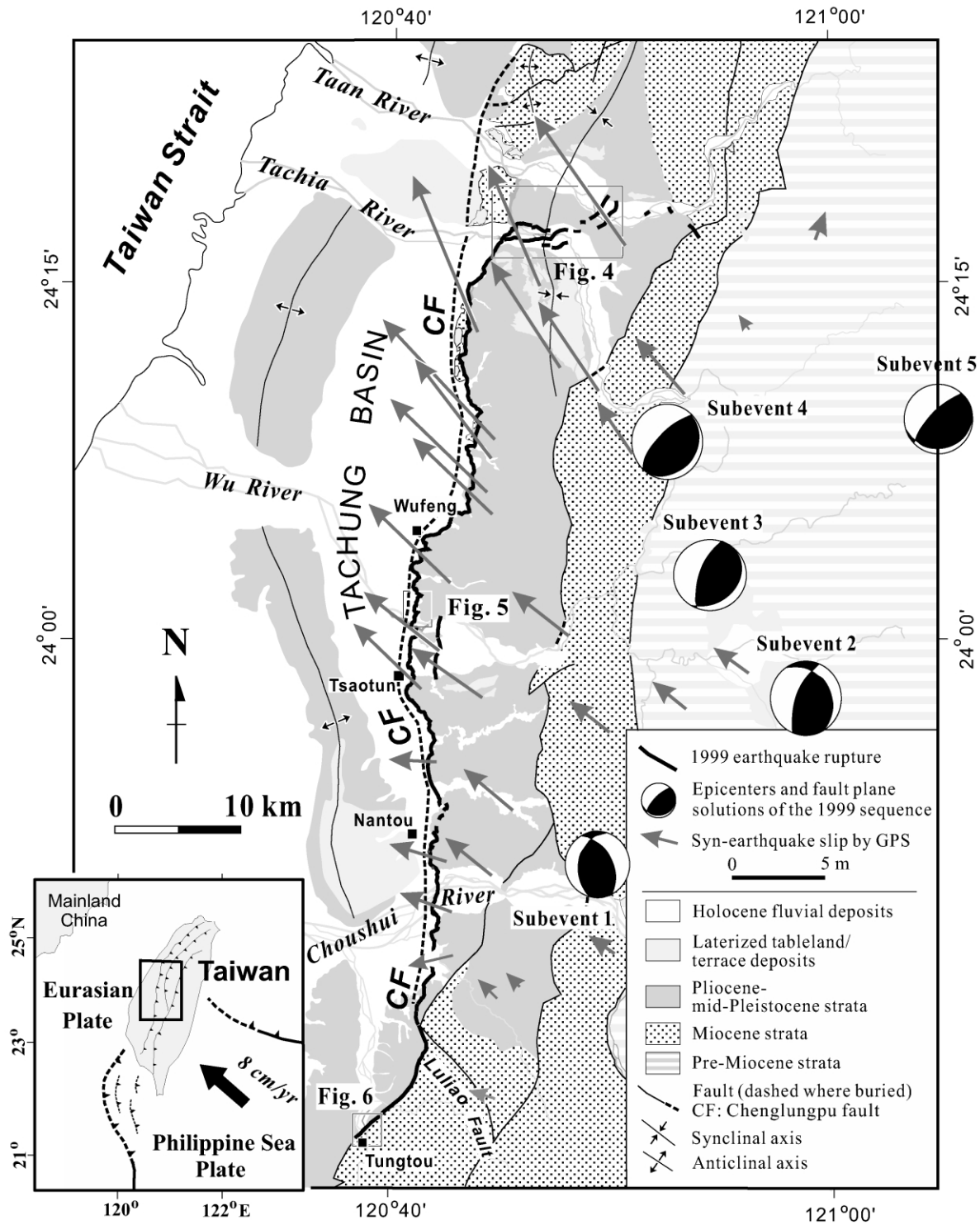

Fig. 1. Geological map of central Taiwan (modified from Chinese Petroleum Corporation (1974, 1982, 1986)), location of the surface rupture during the 1999 Chi-Chi earthquake (based on Central Geological Survey (1999)), syn-earthquake slip revealed by GPS measurements on the hanging-wall side of the rupture (summarized from Yu et al. (2001)) and epicenters of the earthquake sequence (in equal-area projection with the compressional quadrants darkened; after Kao and Chen (2000)). Inset shows map location and tectonic setting of Taiwan. Bold arrow with rate shows the current movement of the Philippine Sea plate relative to the Eurasian plate (Yu et al., 1997).

2. Regional setting and the 1999 Chi-Chi earthquake

2.1. Geological setting

The 1999 Chi-Chi earthquake was due to slip on the Chelungpu fault—a major north-striking thrust fault in the fold-thrust belt in western Taiwan (Fig. 1). The fault thrusts Miocene to mid-Pleistocene sedimentary rocks on the hanging wall over Quaternary conglomerate on the footwall (Chang, 1971) and roughly coincides with the mountain front that defines the eastern margin of the Taichung basin (Fig. 1). The strata on the hanging-wall side of the Chelungpu fault generally dip at 20–30° to the east but >40° near the fault (Chinese Petroleum Corporation, 1974, 1982). These strata are truncated to the south by secondary faults, including the NW-trending Luliao fault, in the Choushui River basin (Fig. 1). From here, the Chelungpu fault (or the Tachienshan fault of Chinese Petroleum Corporation (1986)) enters the hills and bends southwestward (Fig. 1).

2.2. Trace of the surface rupture

The rupture extends from the Taan River in the north to the Chingshui River (tributary of the Choushui River) in the south (note that, for simplicity, we collectively term all the coseismic deformation resulting in recognizable offset in the field as rupture, although in many places it is expressed as a flexure without breaking the surface). About 60% of this rupture (and its secondary branches) is located within a few hundred meters from the mountain-front escarpment bounding the Taichung basin (Fig. 1). In the north, the rupture bends to the east away from the mountain front (and the Chelungpu fault) at the mouth of the Tachia River valley (Fig. 1). From here, the rupture diverges into several subparalleling branches, accompanied by a 1–2-km-wide fold belt, and continues northeastward to the Taan River valley (Fig. 1). In the south, the rupture enters the hills about 4 km south of the Choushui River valley, continuously follows the Chelungpu fault (or the Tachienshan fault), and ends around Tungtou (Fig. 1). In the hills south of the Choushui River valley, the earthquake also generated secondary ruptures, en échelon-aligned domes and abundant landslides along the Luliao fault for several kilometers.

2.3. Geophysical data

Using high-quality teleseismic records, Kao and Chen (2000) divided the main shock of the 1999 earthquake into five successive subevents, each representing the average properties of a portion of the fault rupture at depth (Fig. 1). The rupture initiated about 15 km east of the mouth of the Choushui River valley on a fault plane dipping 50° to the east (Subevent 1; Fig. 1). The rupture then propagated northward along a dominant, 20–30° east dipping plane down to a depth of about 15 km (Subevents 2–4; Fig. 1). Finally, the rupture shifted eastward beneath the high mountainous area about 35 km east of the mountain front

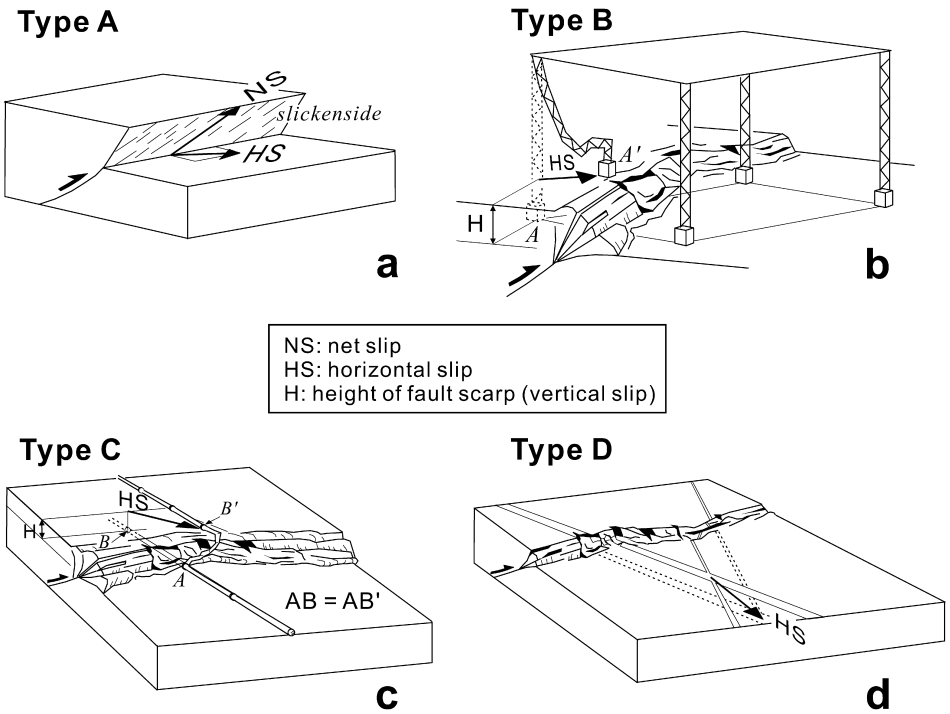

Fig. 2. Four types of objects surveyed in this study (schematic). Type A is bedrock-bounded fault plane exposed on a fault scarp or in a trench. Type B is an object that was translated during faulting. As shown, the roof of the structure remained intact, which allows us to restore the steel rack A′ to its original position A to obtain the slip vector of the rupturing. Type C is an offset linear feature with original length (AB′) preserved. Type D is a pair of the nearby, non-parallel linear features.

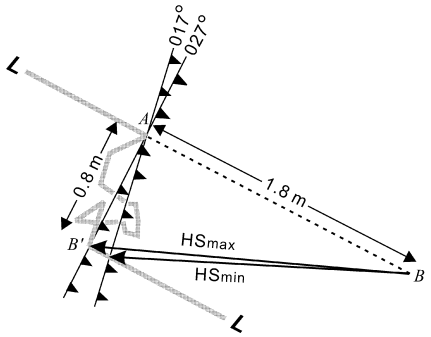

Site A5

(120°49'29"; 24°17'59")

Taan River valley;
L: concrete ditch

Field survey:

Fault azimuth: 017°-027°
L azimuth: 118°
Apparent lateral offset:
0.8 m (right-lateral)
L shortened, AB': 1.8 m
H: 5.5 m

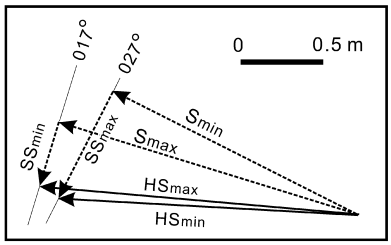

Calculation:

Horizontal slip azimuth:
273°(HSmin)-275°(HSmax)
Horizontal slip:
1.8 m (HSmin)-2.0 m (HSmax)
Maximum shortening (Smax):
1.9 m (component of HSmax in 287°)
Minimum shortening (Smin):
1.6 m (component of HSmin in 297°)
Maximum strike slip (SSmax):
0.8 m (component of HSmin in 307°)
Minimum strike slip (Ssmin):
0.4 m (component of HSmax in 197°)
Net slip: 5.8-5.9 m
Fault dip angle: 71°-74°

Net slip = $(HS^2 + H^2)^{1/2}$

Fault dip angle = $\tan^{-1}(H/S)$

HS: Horizontal slip
H: Height of fault scarp
S: Shortening

a

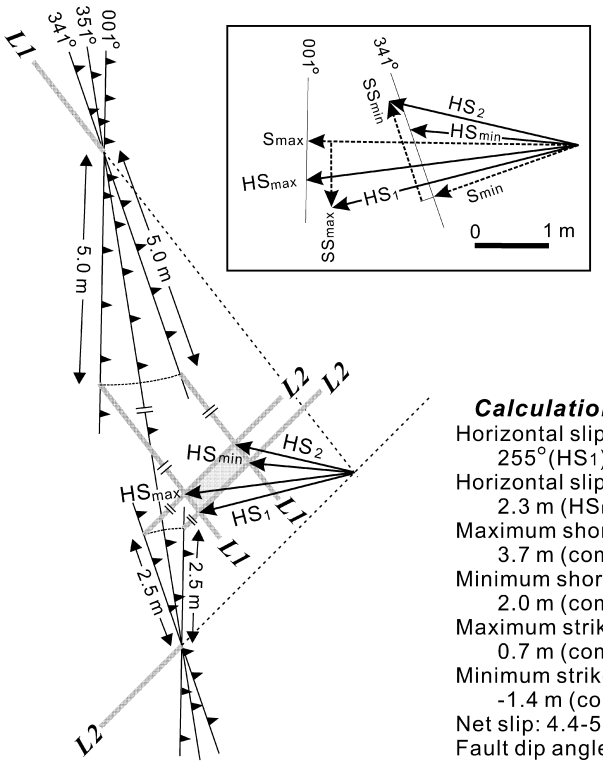

Site D6

(120°42'06"; 23°49'38")

Choushui River valley;
L1, *L2*: ridge in tea farm;
Distance of *L1*, *L2* along fault strike is about 20 m

Field survey:

Fault azimuth: 341°-001°
L1 azimuth: 142°
Apparent lateral offset of *L1*:
5.0 m (right-lateral)
L2 azimuth: 045°
Apparent lateral offset of *L2*:
-2.5 m (left lateral)
H: 3.8 m

Calculation:

Horizontal slip azimuth:
255°(HS1)-283°(HS2)
Horizontal slip:
2.3 m (HSmin)-3.7 m (HSmax)
Maximum shortening (Smax):
3.7 m (component of HSmax in 271°)
Minimum shortening (Smin):
2.0 m (component of HSmin in 251°)
Maximum strike slip (SSmax):
0.7 m (component of HS1 in 181°)
Minimum strike slip (Ssmin):
-1.4 m (component of HS2 in 341°)
Net slip: 4.4-5.3 m
Fault dip angle: 46°-54°

b

Fig. 3. Examples of determining slip vectors and other faulting parameters from (a) type C and (b) type D objects on graphs; fault azimuths are assumed to have uncertainties of ± 5° and ± 10° in (a) and (b), respectively. In (a), the linear feature (L) is almost perpendicular to the fault trace, and its position on the graph is less affected by the irregularity of the fault trace. This results in a small uncertainty in slip azimuth. In (b), the linear feature (L1) makes a small angle with the rupture and its position on the graph is sensitive to the uncertainty of the azimuth of the rupture. This yields a greater uncertainty in slip azimuth (shaded parallelogram).

(Subevent 5; Fig. 1). In this sequence, the slip on the rupture rotated from southwest-west (*P*-axis: 79°) in the south (Subevent 1) to northwest in the region east of Wufeng (Subevent 4) and then to due north (Subevent 5) (Fig. 1). The amount of the slip also increased northward to a maximum of 10 m near the Tachia River valley (Mori and Ma, 2000). Here, the strong-motion records documented the maximum vertical offset of 8 m (Ma et al., 2001).

Near where the surface rupture ended, the aftershock sequences defined two strike-slip nodal planes (Kao and Chen, 2000): the ENE-trending right-lateral plane in the north and the NW-trending left-lateral plane in the south. These data indicate that the main rupture ended laterally in strike-slip fault zones that accommodated the westward slip of the thrust block (Kao and Chen, 2000).

The coseismic slip of the thrust block shown by GPS surveys was dominantly toward the northwest (except for a SW-directed slip south of the Choushui River valley) (Yu et al., 2001) (Fig. 1). The slip rotated counter-clockwise to the north and increased in amount both to the north and to the west, with a maximum of 9.1 m in the area several kilometers south of the Tachia river valley (Fig. 1). The GPS data also showed that the region on the footwall side of the rupture consistently slipped to the southeast or to the east during the earthquake. This slip (0.1–1.5 m) is much smaller than the slip of the thrust block on the hanging-wall side (Yu et al., 2001).

3. Methods

We focused our study on determining the slip vector (including azimuth, amounts of vertical and horizontal slips), shortening, strike-slip component and fault dip-angle of the rupture. All measurements were made in the hanging wall relative to the footwall. The vertical slip (i.e. the height of a fault scarp) is the most readily measured element. It is defined as the vertical distance between the level part of the hanging-wall surface (i.e. behind pressure ridges, if any) and the base of the fault scarp (Fig. 2b and c). For the other faulting parameters, four types of objects were surveyed. Type A objects are the bedrock-bounded fault planes

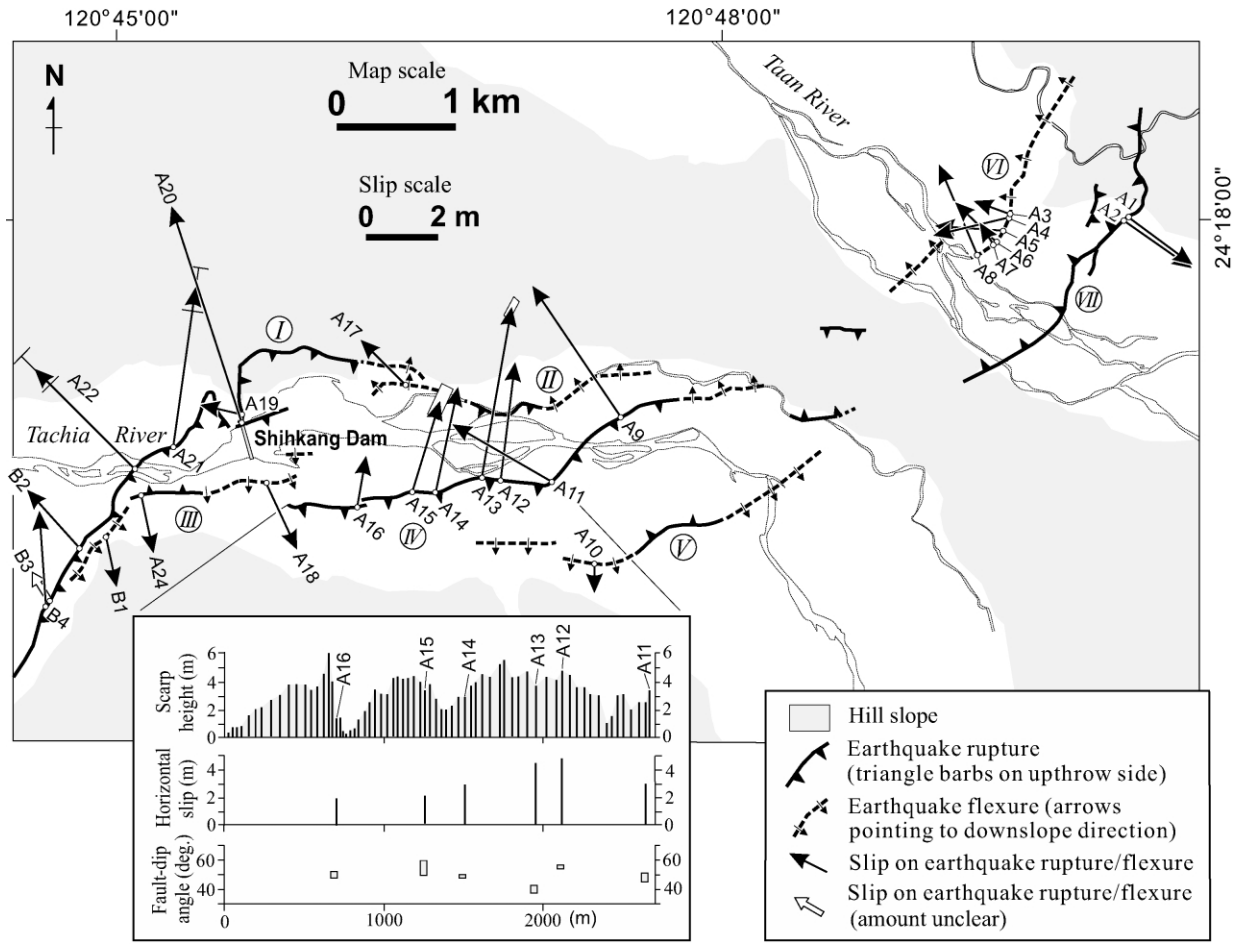

Fig. 4. Surveyed slip vectors in the Taan and Tachia river valleys (for location see Fig. 1). Earthquake ruptures (and flexures) are modified from Central Geological Survey (1999). Surveyed fault-scarp height, horizontal slip and fault dip-angle along the western part of fault IV are also shown. Uncertainties of $>10°$ in slip azimuth or >0.5 m in horizontal slip are given as parallelograms or thin bars. Letters with numbers refer to the number of survey sites shown in Appendix A.

exposed on fault scarps or in trenches (Fig. 2a). We directly measured the fault plane attitudes and determined the slip azimuths from slickensides. Type B objects are those, such as equally spaced building pillars, that were translated during the earthquake (Fig. 2b). We obtained the slip vectors by restoring the objects to their original positions. Type C objects are offset linear features such as city streets or concrete fences. These objects are rigid and the lengths before the faulting can be readily measured, which allowed us to calculate slip vectors of the rupture (Fig. 2c). In some places, the original lengths of the objects are unknown. Still, we obtained slip azimuths where the objects were offset only vertically. Type D objects are pairs of nearby, non-parallel linear features that were offset by the rupture (Fig. 2d). We were rarely able to directly determine slip vectors from types C and D objects in the field. Instead, we measured the azimuth of the rupture, the azimuths and apparent lateral offsets of the objects, and determined the slip vectors graphically (Fig. 3).

Our measurements have differing degrees of uncertainty for each type of object and are affected by the orientations of the objects with respect to the rupture. The direct measurement of fault attitude and/or slip azimuth from type A and B objects is the most accurate. Where the exposed fault plane of Type A object is irregular, we measured more than one value to obtain the range of the fault attitude and slip azimuth.

For type C and D objects, we found that the differences in orientation between the offset linear features on the hanging-wall side of the fault and their counterparts on the footwall side are all within 1 or 2° (i.e. almost no near-surface rotation on the rupture). These measurements, together with those for lateral offsets of the linear features and heights of fault scarps, can be assumed to be precise. The major source of uncertainty is in determining the azimuth of the fault trace, which is usually a ruptured zone rather than a perfectly straight line on the field scale. We assume that our measured fault azimuth has an uncertainty of $\pm 5°$ where the fault trace appears to be straight, and of $\pm 10°$ when the fault trace is rather irregular or is composed of multiple closely-spaced branches. This yields uncertainty in determining the positions of the offset objects on the graphs (Fig. 3). The obtained slip azimuth thus can have an uncertainty of over 20° where the fault has a large strike-slip component or where the offset linear feature makes a small angle with the fault (Fig. 3). This uncertainty can also result in uncertainties in determining shortening and strike-slip component (and thus fault-dip angle) of over 50%. Fig. 3

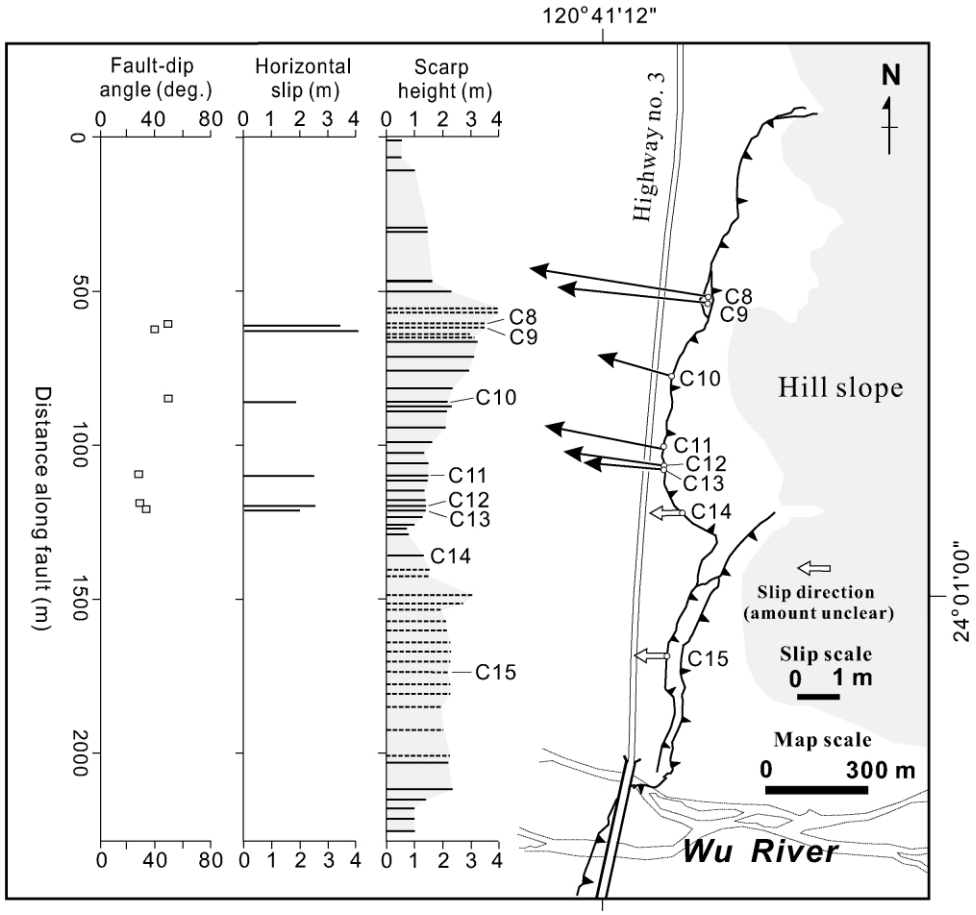

Fig. 5. Surveyed slip vectors on the earthquake ruptures north of the Wu River valley (for location see Fig. 1). Bars for vertical slip are dashed where they are the summation of the heights of two nearby fault scarps. Legend and other notes as in Fig. 4.

shows examples of how we determined the faulting parameters and their possible ranges, given the uncertainties of fault azimuths.

4. Results

4.1. Local variations

Our obtained faulting parameters show significant local variations, from which we were able to appreciate the complexity of the near-surface reverse-faulting processes. The faulting patterns are especially complicated where the rupture is irregular in traces and is associated with flexure. For example, along the northwestern branch of the rupture in the Taan River valley (Fault VI; Fig. 4), a total of six measured slip vectors vary from 256 to 341° in azimuths in a distance of 500 m. The net slips of these vectors also vary from 1.0 to 5.9 m, and fault dip-angles from 14 to 74°.

In some places the trace of the rupture is relatively straight and the measured slip-azimuths are consistent. Still, the fault-scarp heights and horizontal slips oscillate along the rupture, with wavelengths of several hundred meters to 1 km. Examples of this case are shown on the rupture on the southern bank of the Tachia River (Fault IV; Fig. 4) and the rupture north of the Wu River (Fig. 5). In both places, the fault-scarp heights and their correspondent horizontal slips appear to show positive correlations (Figs. 4 and 5). However, the measured fault dip-angles show as much as 20° variations (Figs. 4 and 5), which make the prediction of horizontal slips from known fault-scarp heights imprecise. The complexity of faulting processes is also shown on ruptures that are dominated by lateral slips. The rupture in Tungtou is an example (Fig. 6). Here, although the rupture is straight and has a relatively uniform height, the lateral slip changes by 2.4 m in a distance of 40 m (Fig. 6).

Our observed local variations of faulting parameters suggest that the rupture is composed of multiple segments,

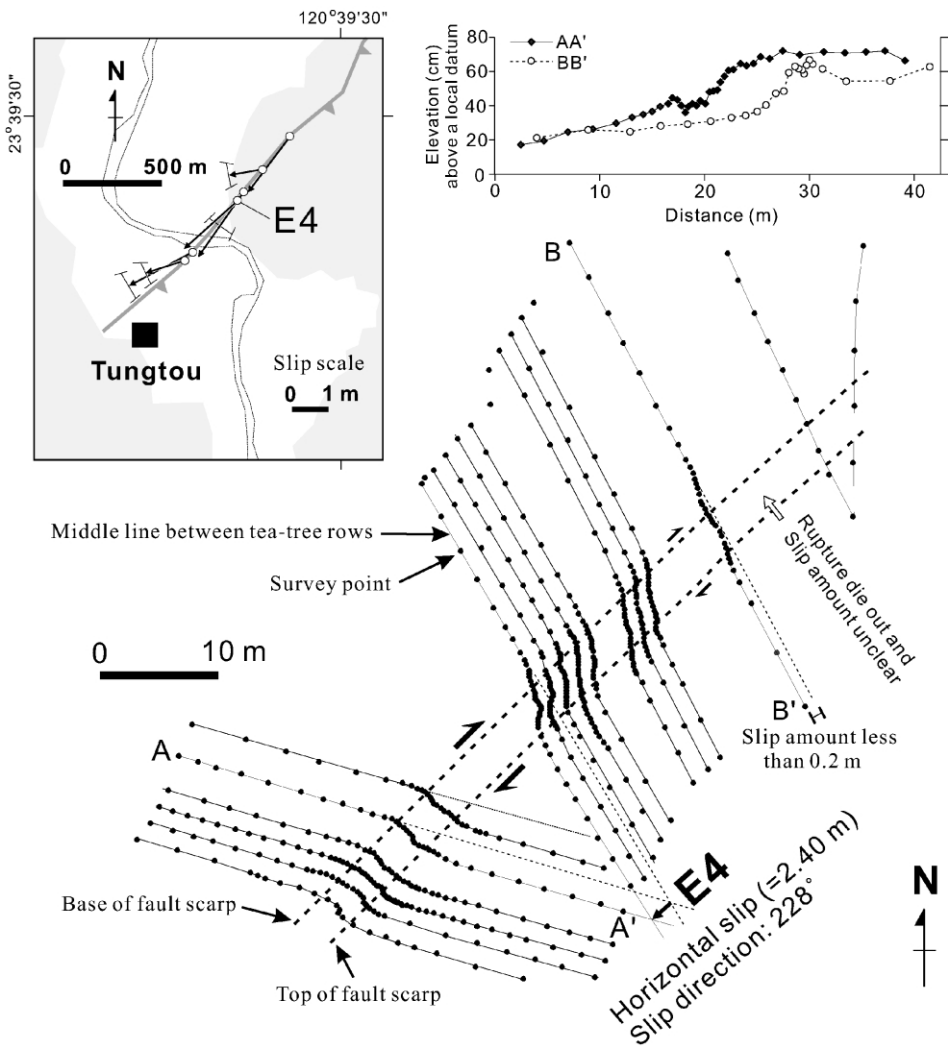

Fig. 6. Deformation of a tea farm near Tungtou. The middle lines between two rows of tea trees were surveyed by total station to document the detailed characteristics of the faulting. Inset (for location see Fig. 1) shows location (E4). Legend and other notes as in Fig. 4. Note the local change of horizontal slip vector, although the fault scarp appears to be straight and has a relatively uniform height.

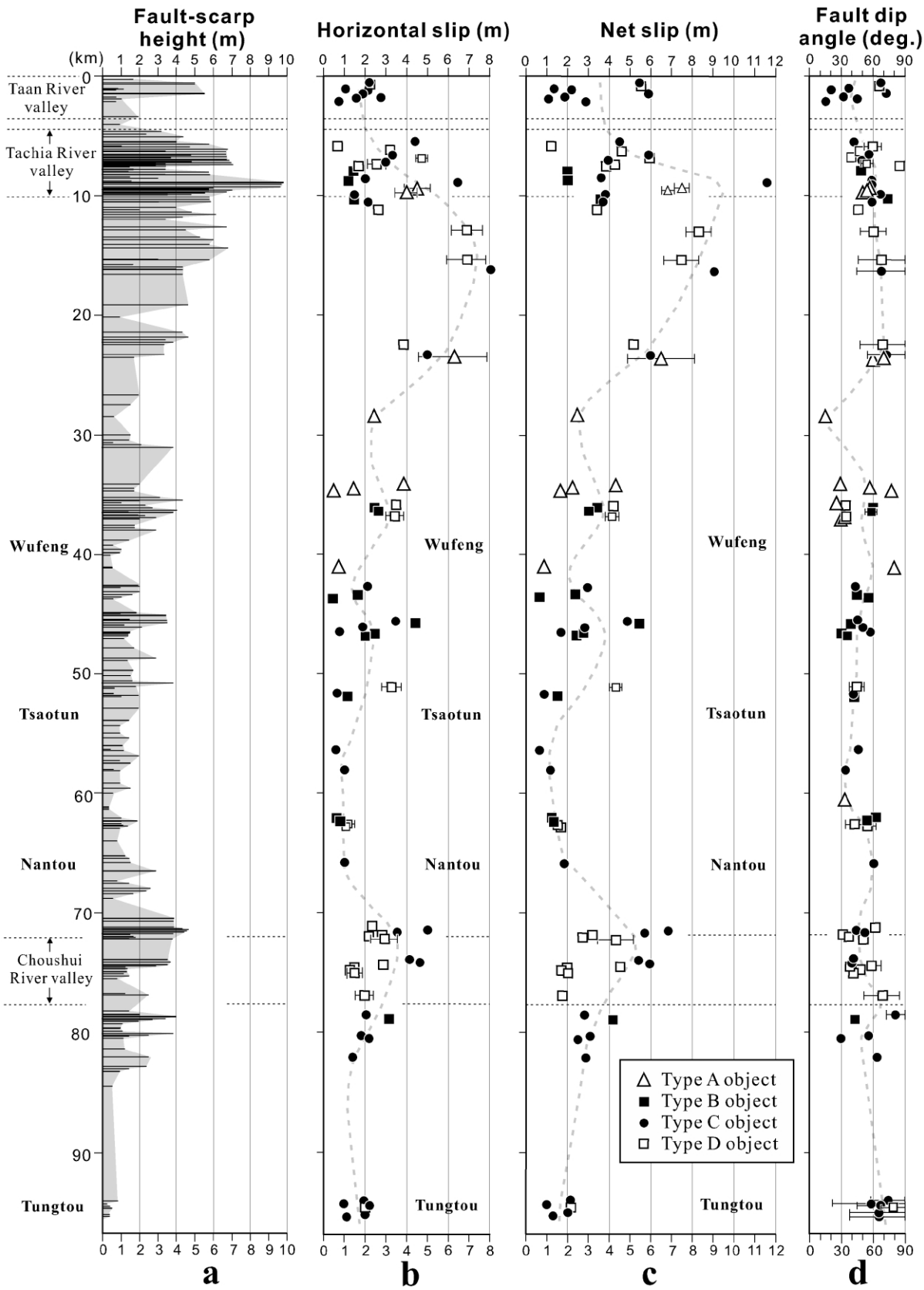

Fig. 7. Results of our surveyed faulting parameters. Longitudinal axis is distance from north to south along the earthquake rupture except for the Taan and Tachia river valleys, in which the distance is along the mid-line of the uplifted zone.

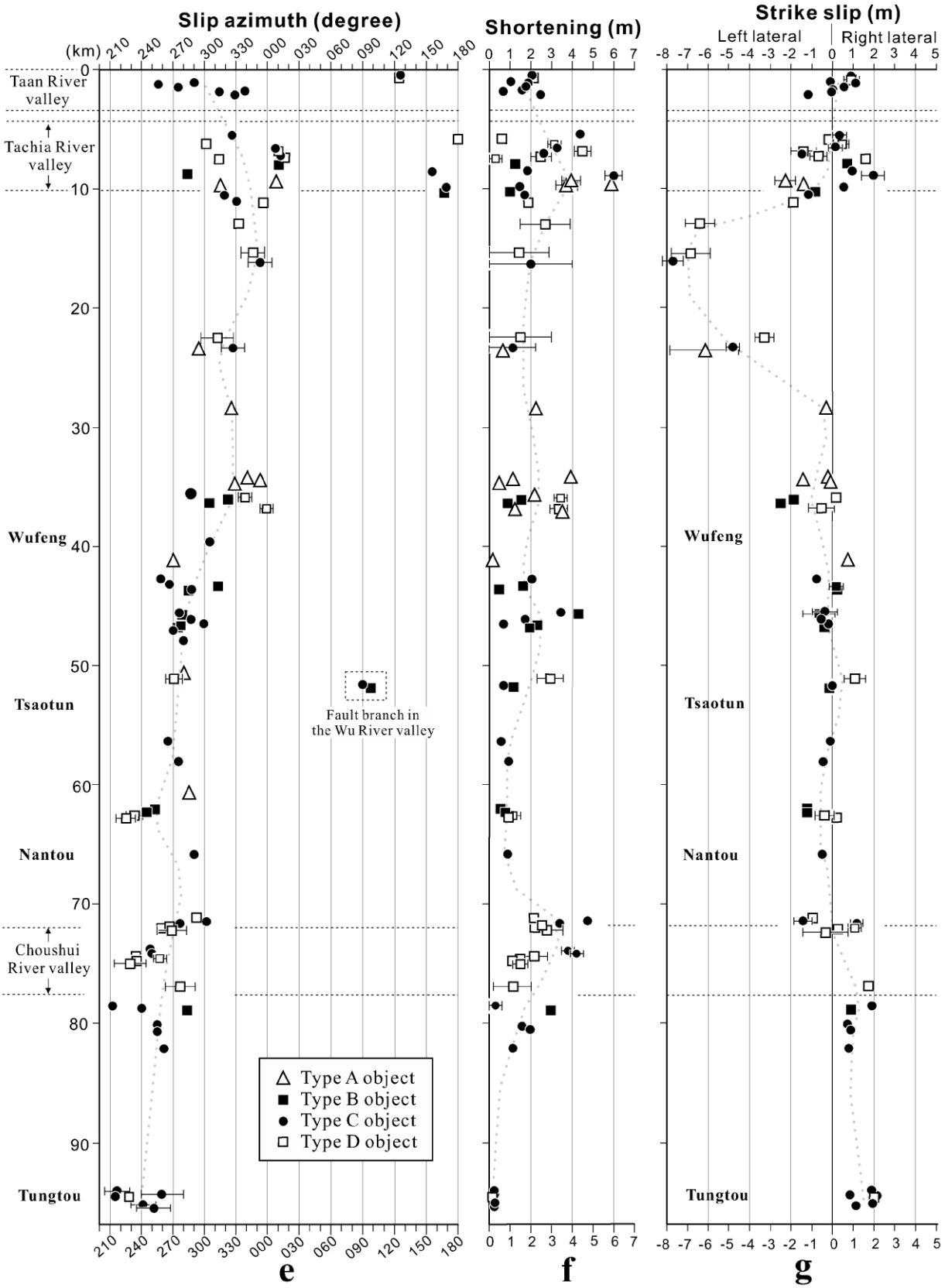

Fig. 7 (*continued*)

even if it appears to be continuous or uniform on a broader scale. The origins of these diversities have yet to be made clear. This nonetheless highlights the importance of survey quantity to reduce potential bias upon regional patterns of the faulting parameters.

4.2. Regional patterns

(1) *Vertical slip*. We obtained more than 300 values of fault-scarp height (Fig. 7a). They are greater (maximum: 10 m) in the Taan and Tachia river valleys, decrease to the south (<4.5 m), and appear to have lower values (<2 m) in Tsaotun-Nantou and around Tungtou (Fig. 7a).

(2) *Horizontal slip*. Horizontal slip varies from <1 to 6.5 m along the fault branches in the Taan and Tachia river valleys (Figs. 4 and 7b). The values reach a maximum of 8 m about 6 km south of the mouth of the Tachia River valley (Fig. 7b). From here to the south, the horizontal slip is generally less than 4 m and appears to have lower values (<2 m) in Tsaotun-Nantou and around Tungtou (<2.5 m) (Fig. 7b).

(3) *Net slip*. The pattern of net slip is similar to those of vertical and horizontal slips, with the maximum (12 m) around the mouth of the Tachia River valley and the minimum (<1 m) in Tsaotun-Nantou and around Tungtou (Fig. 7c). The overall net slip also is statistically well correlated with both vertical and horizontal slips (Fig. 8a and b).

(4) *Fault dip-angle*. Fault dip-angle varies from 15 to 90° (minimum on a minor fault branch 10 km north of Wufeng), and may appear to be smaller (<60°) in Wufeng-Nantou (Fig. 7d). This great variation reflects the fact that, although both well correlated with net slips, the correlation between vertical and horizontal slips is poor even removing the slips that have dominant lateral components (Fig. 8c).

(5) *Slip azimuth*. Slip vector bounding either side of the uplifted zone in the Taan River valley strikes oppositely—west/northwest (256–341°) on the northwestern side (Fault VI) and southeast (about 125°) on the southeastern side (Fault VII) (Figs. 4 and 7e). In the Tachia River valley, the slip vector may be divided into two groups: one generally N–S oriented (153–182° for Faults III and V and 005–019° for the western part of Fault IV), another NW-directed (298–326° for Fault II and the eastern part of Fault IV) (Fig. 4). From here to the south, the slip appears to rotate counter-clockwise, striking from north-northwest (315–011°) at the mouth of the Tachia River valley to roughly west (257–316°) in Wufeng-Tsaotun and to southwest (205–280°) around Tungtou (Fig. 7e).

(6) *Shortening*. Shortening is greater in the Tachia River valley (maximum 6 m, near the valley mouth; Fault I, Fig. 4), between Wufeng and Tasotun (maximum 4.2 m) and around the Choushui River valley (maximum 4.8 m) (Fig. 7f). As the pattern of vertical and horizontal slips, the shortening is smaller in Tsaotun-Nantou (<2 m) and around Tungtou (<1 m) (Fig. 7f).

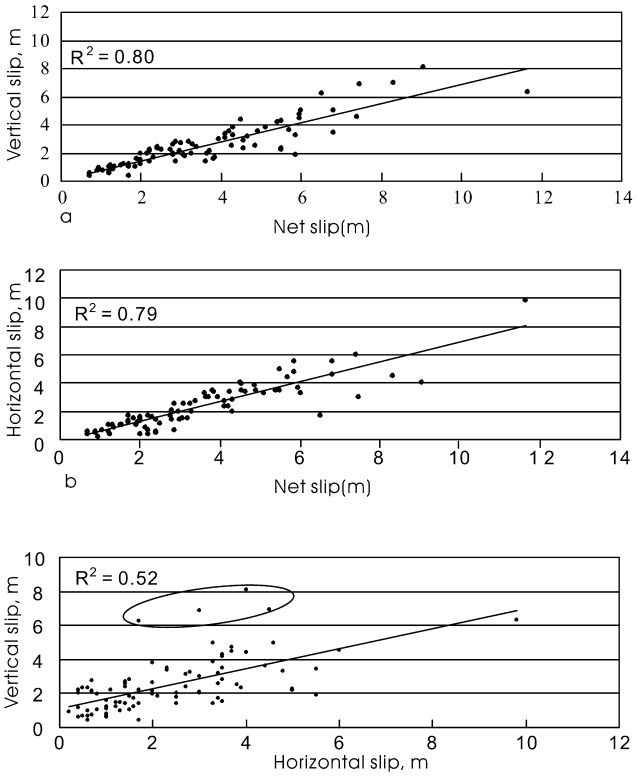

Fig. 8. Plots of (a) fault-scarp height versus net slip, (b) horizontal slip versus net slip, and (c) horizontal slip versus fault-scarp height (R square not taking the four left-lateral slips south of the Tachia River valley into account).

(7) *Strike slip*. Most slip consists of either right-lateral or left-lateral components of generally <2 m (Fig. 7g). Significantly larger left-lateral slip (up to 7–8 m) occurs between the Tachia River valley and Wufeng (Fig. 7g). In contrast, right-lateral slip dominates south from the Choushui River valley (Fig. 7g).

4.3. Deformation mechanism

Our faulting parameters were used to determine the deformation mechanism of the rupture (Fig. 9). The dominantly W-directed slip between Wufeng and the Choushui River valley was generally perpendicular to the strike of the rupture and was therefore characterized by pure thrusting. In this region, large net slips (up to 6.8 m) and shortenings (up to 4.8 m) occurred in Wufeng-Tsaotun and in the Choushui River valley. To the north, the slip rotated to the northwest and to the north, and increased in amount. These NW-/N-directed slips resulted in the maximum left-lateral strike slip (8 m) on the N-striking rupture south of the Tachia River valley. Farther north, accompanyed by the bending of the rupture to the east, the NW-/N-directed slips in the Taan and Tachia River valleys were characterized by pure thrusting, with the maximum horizontal and vertical slips (6.5 m and 10 m, respectively) and shortening (6 m) occurring near the mouth of the Tachia River valley. South of the Choushui River valley, the rupture was characterized

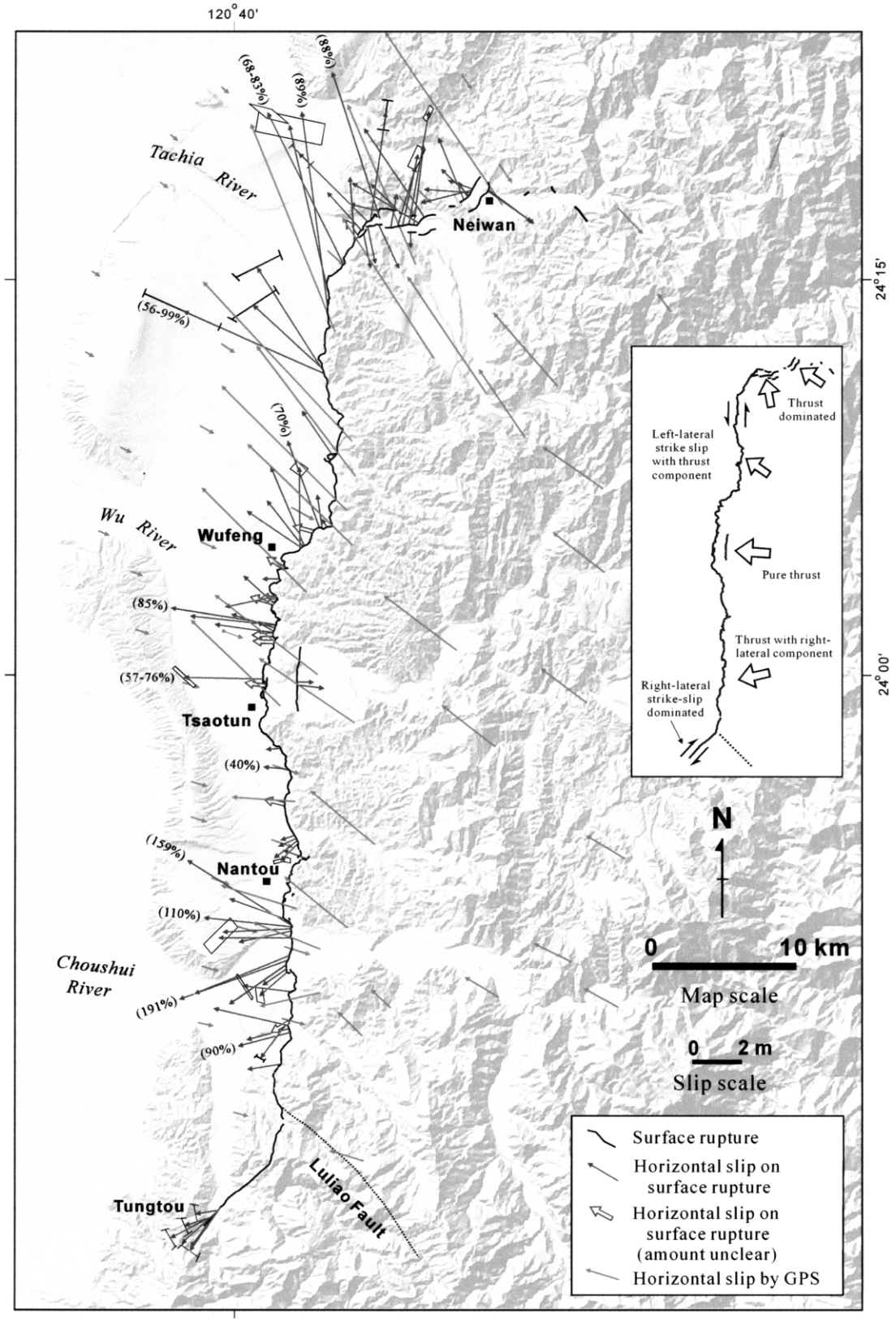

Fig. 9. Comparison between horizontal slip surveyed in this study and slip of the thrust block by GPS. Percentage (in parenthesis) adjacent to slip vector on the rupture is the proportion of the slip to the slip recorded at the nearest GPS station on the hanging-wall side of the rupture (projected to the same azimuth). Legend and other notes as in Figs. 1 and 4. Note the apparent discrepancy between the slip on the earthquake rupture and the slip by GPS south of the Choushui River valley. Inset summarizes the deformation mechanism of the surface rupture.

by oblique, SW-directed thrust with a right-lateral component (maximum: 1.9 m). The right-lateral slips (maximum: 2.4 m) dominated at the southern end of the rupture (striking northeast) near Tungtou.

5. Discussion and conclusions

5.1. Discrepancy with GPS data

Our data are consistent with the seismological and GPS data in that the slip vector of the earthquake rupture progressively rotates and increases in amount to the north (Fig. 9; Kao and Chen, 2000; Mori and Ma, 2000; Yu et al., 2001). We obtained the maximum values of horizontal slip south of the Tachia River valley, which is the place where the maximum slip was recorded by GPS. Also, the fault scarp is higher in the north. This is consistent with the GPS data (Yu et al., 2001) and is comparable with those from near-source strong motion records (Ma et al., 2001).

Our measured slip vectors, however, appear to cover a wider range of azimuth than the slip revealed by GPS surveys (i.e. the slip on the rupture makes a greater rotation from one end to the other end of the rupture than the entire thrust block) (Fig. 9). This difference is particularly shown in the area south of the Choushui River valley where the dominantly W-/SW-directed slips on the rupture are only locally recorded at a GPS station (Fig. 9). Yu et al. (2001) suspected that the data recorded at this station might involve artificial errors. Our data, however, argue that this may not be the case, and that the area slipped to the southwest during the earthquake.

It is possible that we missed measuring some horizontal slips that are greater than our measurements (for example, not all of our measurements were made on the rupture that has local maximum scarp heights). Also, there likely exist coseismic folds or minor, undetected thrust faults behind the rupture. Given these, it is expected that our obtained horizontal slip should not be greater than the slip recorded at GPS stations that are away from the rupture. Indeed, all of our obtained horizontal-slip values north of the Choushui River valley are smaller than those recorded at GPS stations (Fig. 9). The area south of the Choushui River valley, however, shows different results. Here, not only are the azimuths inconsistent as mentioned above, but many of our horizontal-slip measurements are larger than the slip values from nearby GPS stations (Fig. 9). This is true even considering the slip recorded at the GPS stations on the footwall side (<1 m; Fig. 9) for the total slip across the rupture.

We suspect that this discrepancy could reflect the differential movement of the thrust block during the earthquake sequences (Fig. 10). As shown by the seismological data (Fig. 1), the thrusting initiated in the south (to southwest-west) and progressively rotated and propagated to the north (Kao and Chen, 2000). We propose that under

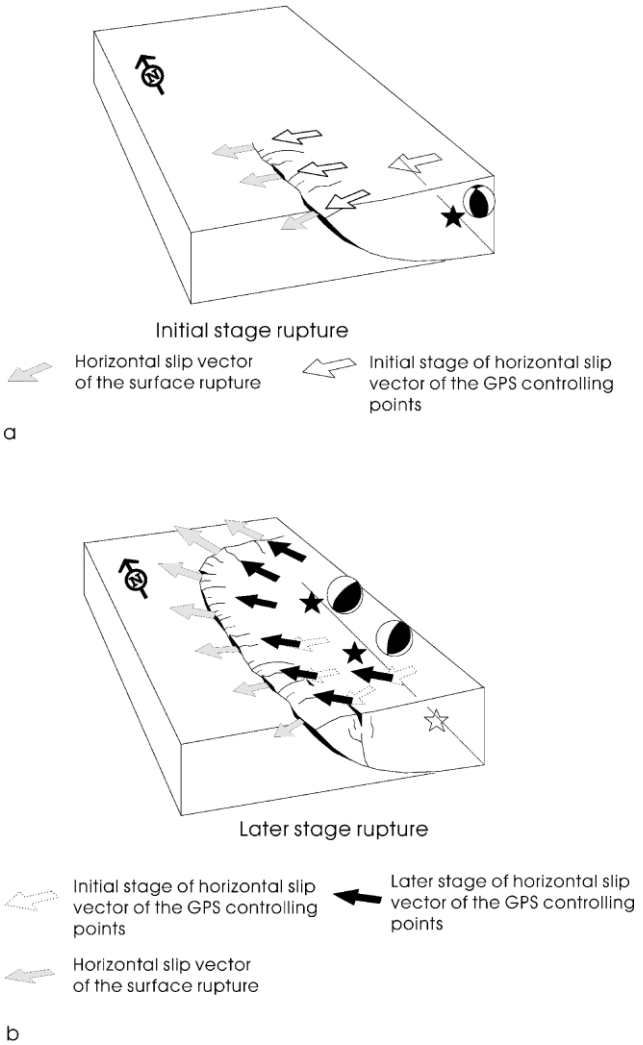

Fig. 10. Cartoon showing the proposed deformation sequence of the thrust block during the 1999 Chi-chi earthquake. (a) The southern part of the thrust block moved to the west/southwest (Subevent 1 in Fig. 1). (b) As the rupture propagated northward (Subevents 2–4 in Fig. 1), the entire thrust block was drawn to the northwest. The GPS data surveyed away from the surface rupture record the accumulated slip of this sequence. The slip on the surface rupture, however, was unlikely to rotate after the movement. This results in the contrast between our measured slip azimuth (and amount) and that by GPS in the southern part of the thrust block.

this process much of the thrust block in the south had rotated and moved to the north after its initial SWW-directed motion (Fig. 10). The accumulated slips of this movement were recorded by GPS, which was surveyed on the thrust block away from the surface rupture (i.e. where the thrust block is relatively thick). In contrast, it is unlikely that any rotation of the thrust block could have occurred on the surface rupture, which is irregular and apparently has greater friction. In other words, our measured slip vectors are likely to record only the initial movement of the thrust block (Fig. 10). This explains why the measured slip azimuths along the southern part of the rupture are more consistent with the seismological data (i.e. Subevent 1) than GPS data. Also, in this region, as the interior thrust block,

Table 1

Site no.[a]	Long. (E)	Lat. (N)	Type (Fig. 2)	Fault azimuth (°)	Vertical slip (m)	Hori. slip (m)	Net slip (m)	Fault dip-angle (°)	Slip azimuth (°)	Shortening (m)	Strike slip[b] (m)
A1	120.8341	24.2996	C	235–245	5.0	2.1–2.3	5.4–5.5	66–69	126–127	1.9–2.2	0.7–1.1
A2	120.8341	24.2996	D	235–245	5.0	2.1–2.5	5.4–5.6	64–69	122–128	1.9–2.4	0.6–1.3
A3	120.8247	24.3003	C	009–019	0.8	1.0–1.1	1.3–1.4	36–39	290–291	1.0–1.1	(−0.2)–0.0
A4	120.8245	24.3018	C	011–021	0.7	2.1–2.2	2.1–2.3	19–22	256–257	1.7–2.0	0.9–1.3
A5	120.8235	24.2998	C	017–027	5.5	1.8–2.0	5.8–5.9	71–74	273–275	1.6–1.9	0.4–0.8
A6	120.8234	24.2995	C	055–065	1.0	1.6	1.9	32	314	1.6	(−0.1)–0.1
A7	120.8220	24.2981	C	051–061	0.7	0.7–0.8	1.0–1.1	41–49	325–332	0.6–0.8	(−0.1)–0.0
A8	120.8213	24.2975	C	038–048	0.7	2.6–2.9	2.7–3.0	14–18	335–341	2.2–2.7	(−1.4)–(−1.0)
A9	120.7903	24.2840	C	055–065	4.0	4.4	4.5	42–43	326	4.3–4.4	0.0–0.7
A10	120.7900	24.2740	D	240–260	1.0	0.5–0.8	1.1–1.3	51–68	178–182	0.4–0.8	(−0.3)–(−0.1)
A11	120.7871	24.2807	D	040–050	3.4	3.0–3.4	4.5–4.8	45–51	298–304	2.8–3.4	0.2–0.8
A12	120.7819	24.2805	C	095–105	4.8	3.2–3.4	5.8–5.9	55–57	006–009	3.1–3.4	(−0.2)–0.5
A13	120.7810	24.2805	D	078–088	3.7	4.4–5.0	5.7–6.2	37–42	009–011	4.1–4.9	(−2.0)–(−0.8)
A14	120.7780	24.2800	C	065–075	3.0	3.0	3.9–4.0	48–50	012	2.5–2.7	(−1.6)–(−1.4)
A15	120.7750	24.2796	D	087–097	3.4	2.1–3.0	4.0–4.5	49–60	015–019	2.0–3.0	(−1.1)–(−0.3)
A16	120.7700	24.2787	B	065–075	1.4	1.4	2.0	47–52	010	1.1–1.3	0.6–0.8
A17	120.7749	24.2879	D	119–129	3.4	1.5–1.9	3.7–3.9	80–90	310–318	0.0–0.6	1.5–1.8
A18	120.7619	24.2804	C	270–280	3.0	1.9–2.1	3.6–3.7	56–62	153–158	1.6–2.0	0.8–1.1
A19	120.7604	24.2858	B	–	1.6	1.2	2.0	–	283	–	–
A20	120.7605	24.2844	C	085–095	9.8	6.1–6.5	11.5–11.8	57–60	341–343	5.6–6.4	1.4–2.5
A21	120.7528	14.2822	A	068	6.0	3.9–5.1	7.1–7.9	54–60	005–011	3.5–4.3	(−2.8)–(−1.8)
A22	120.7528	24.2822	A	024	5.5	3.4–4.5	6.5–7.1	51–58	315	3.2–4.2	(−1.6)–(−1.2)
A23	120.7572	24.2860	A	065	7.0	–	–	50	–	5.9	–
A24	120.7520	24.2790	C	270–280	3.5	1.5–1.6	3.8	67–68	168–169	1.4–1.5	0.3–0.6
B1	120.7490	24.2760	B	031–041	3.3	1.4	3.6	73	168	1.0	(−0.9)
B2	120.7469	24.2743	C	325–335	3.0	1.9–2.3	3.6–3.8	57–62	318–319	1.6–1.9	(−1.3)–(−1.1)
B3	120.7447	24.2713	C	020–040	4.0	–	–	–	330	–	–
B4	120.7445	24.2711	D	037–047	2.0	2.5–2.8	3.2–3.4	44–50	353–359	1.7–2.1	(−2.1)–(−1.8)
B5	120.7372	24.2560	D	345–355	4.5	6.2–7.7	7.7–8.9	49–72	330–337	1.5–3.9	(−7.1)–(−5.7)
B6	120.7284	24.2379	D	340–000	3.0	5.9–7.8	6.6–8.3	46–90	335–358	0.0–2.9	(−7.8)–(−5.9)
B7	120.7260	24.2370	C	350–010	4.0	7.9–8.3	8.9–9.2	45–90	341–004	0.0–4.0	(−8.2)–(−7.2)
B8	120.7268	24.1750	D	323–343	3.3	3.6–4.1	4.9–5.3	48–90	297–328	0.0–3.0	(−3.7)–(−2.8)
B9	120.7258	24.1749	C	323–343	3.3	4.9–5.1	5.9–6.1	55–90	316–339	0.0–2.3	(−5.1)–(−4.5)
B10	120.7254	24.1759	A	300	1.7	4.6–7.9	4.9–8.1	65–75	294	0.5–0.8	(−7.9)–(−4.6)
B11	120.7309	24.1341	A	044	0.6	2.3–2.4	2.3–2.5	15	322–329	2.2	(−0.4)–(−0.2)
B12	120.7169	24.0883	A	065	2.0	3.8	4.3	28	340	3.8	−0.3
B13	120.7231	24.0883	A	045	1.7	1.4	2.2	57	352	1.1	−1.4
B14	120.7280	24.0880	A	045	1.7	0.4	1.7	77	327	0.4	−0.1
B15	120.7144	24.0820	C	065–075	2.0	–	–	–	287	–	–
B16	120.7145	24.0817	A	047	1.0	–	–	25	–	2.1	–
B17	120.7131	24.0788	D	055–065	2.3	3.3–3.7	4.0–4.4	32–37	332–342	3.1–3.7	(−1.0)–0.4
B18	120.7134	24.0791	B	355–005	2.7	2.4	3.4	59–61	322	1.5–1.6	(−1.8)–(−2.0)
B19	120.7136	24.0800	B	319–329	1.4	2.7	3.0	52–63	304	0.7–1.1	(−2.4)–(−2.6)
B20	120.7134	24.0791	D	075–085	2.3	3.0–3.7	3.8–4.4	32–38	353–005	2.9–3.7	(−1.2)–0.1
B21	120.7134	24.0790	A	000	2.0	–	–	30	–	3.5	–
C1	120.0963	24.0630	C	355–005	1.0	–	–	–	305	–	–
C2	120.0930	24.0546	A	082	0.5	0.7	0.9	80	269	0.1	0.7
C3	120.6901	24.0451	C	323–333	2.0	2.1–2.2	2.9–3.0	42–46	257–259	1.9–2.2	(−1.0)–(−0.5)
C4	120.6903	24.0447	C	351–001	2.0	–	–	–	266	–	–
C5	120.6898	24.0411	B	040–060	1.6	1.7	2.3	43–45	312	1.6–1.7	(−0.1)–0.5
C6	120.6898	24.0412	C	035–045	1.0	–	–	–	287	–	–
C7	120.6700	24.0415	B	044–054	0.6	0.4	0.7	56	285	0.4	0.2
C8	120.6896	24.0250	C	350–010	3.5	3.5	4.9	45–46	276	3.4–3.5	(−1.0)–0.2
C9	120.6904	24.0267	B	350–010	3.5	4.3	5.5	39–40	279	4.1–4.3	(−1.4)–0.1
C10	120.6884	24.0200	C	355–005	2.1	1.8–1.9	2.8	49–51	287–288	1.7–1.8	(−0.7)–(−0.4)
C11	120.6883	24.0208	C	008–018	1.5	2.6	3.06	28	299–300	2.25	1.3
C12	120.6884	24.0206	B	355–005	1.4	2.4	2.8	30–31	278	2.3–2.4	(−0.5)–(−0.1)
C13	120.6884	24.0205	B	350–000	1.4	2.0	2.4	36–37	275	1.9–2.0	(−0.5)–(−0.2)
C14	120.6884	24.0207	C	345–355	1.2	–	–	–	270	–	–
C15	120.6883	24.0150	C	015–025	1.7	–	–	–	274	–	–
C16	120.6821	23.9816	D	017–027	2.8	2.8–3.7	4.0–4.6	38–51	263–279	2.3–3.6	0.7–1.6

(*continued on next page*)

Table 1 (*continued*)

Site no.[a]	Long. (E)	Lat. (N)	Type (Fig. 2)	Fault azimuth (°)	Vertical slip (m)	Hori. slip (m)	Net slip (m)	Fault dip-angle (°)	Slip azimuth (°)	Shortening (m)	Strike slip[b] (m)
C17	120.6814	23.9888	C	007–017	1.6	–	–	–	280	–	–
C18	120.7048	23.9775	C	175–185	0.6	0.7	0.9	41	90	0.7	(−0.1)–0.1
C19	120.7045	23.9775	B	175–185	1.0	1.1	1.5	42	97	1.1	(−0.2)–(−0.1)
C20	120.6942	23.9473	C	335–345	0.4	0.6	0.7	34–39	265	0.5–0.6	(−0.2)–(−0.1)
C21	120.6999	23.9346	C	332–342	0.6	1.0	1.2	31–37	274–276	0.8–1.0	(−0.5)–(−0.4)
C22	120.6969	23.9130	A	010	–	–	–	30	285	–	–
C23	120.7005	23.8978	B	305–325	1.0	0.6	1.2	59–63	252	0.5–0.6	(−0.4)–(−0.1)
C24	120.7005	23.8977	B	305–325	1.0	0.8	1.3	51–55	245	0.7–0.8	(−0.4)–(−0.1)
C25	120.7750	23.8976	D	300–320	1.0	0.9–1.5	1.3–1.8	34–51	225–241	0.8–1.5	(−0.8)–0.1
C26	120.7021	23.8956	D	322–332	1.3	0.9–1.2	1.6–1.8	47–62	216–234	0.7–1.2	(−0.1)–0.4
C27	120.7067	23.8760	C	345–355	1.5	1.0–1.1	1.8–1.9	59–62	290	0.8–0.9	(−0.6)–(−0.4)
D1	120.7017	23.8327	D	351–001	3.9	2.2–2.5	4.5–4.6	58–64	292	1.9–2.4	(−1.2)–(−0.7)
D2	120.7021	23.8355	C	010–020	4.6	5.0	6.8	43–45	302	4.6–4.9	(−1.8)–(−1.0)
D3	120.7017	23.8324	C	020–030	4.4	3.6	5.7	51–53	276	3.3–3.5	0.8–1.5
D4	120.7011	23.8311	D	015–025	1.5	2.6–3.0	3.0–3.4	28–34	265–268	2.2–2.8	0.7–1.4
D5	120.7011	23.8308	D	350–000	1.7	2.0–2.4	2.6–2.9	35–40	258–259	2.0–2.4	0.0–0.5
D6	120.7019	23.8275	D	341–001	3.8	2.3–3.7	4.4–5.3	46–54	255–283	2.0–3.7	(−1.4)–0.7
D7	120.6981	23.8098	C	359–009	3.5	4.0–4.3	5.3–5.5	40–45	247–249	3.5–4.1	1.5–2.2
D8	120.6981	23.8097	C	359–009	3.7	4.5–4.9	5.8–6.1	39–43	249–251	3.9–4.6	1.6–2.2
D9	120.6891	23.9095	D	357–017	3.5	2.6–3.1	4.4–4.7	51–68	230–239	1.4–2.8	1.5–2.3
D10	120.6983	23.8081	D	344–354	1.2	1.3–1.7	1.8–2.1	35–43	251–264	1.3–1.7	(−0.3)–0.3
D11	120.6983	23.8080	D	344–354	1.2	1.0–1.4	1.6–1.8	43–53	230–240	0.9–1.3	0.4–0.8
D12	120.6983	23.8074	D	305–315	1.3	1.2–1.8	1.8–2.2	36–47	214–244	1.2–1.8	(−0.7)–0.3
D13	120.7006	23.7936	D	055–075	2.5	1.6–2.4	3.0–3.5	51–85	263–291	0.2–2.0	1.5–2.0
D14	120.7014	23.7772	C	025–035	2.0	1.9–2.0	2.8	73–90	212–223	0–0.6	1.9
D15	120.7026	23.7785	C	345–355	4.0	–	–	–	240	–	–
D16	120.7010	23.7768	B	025–035	2.7	3.1	4.1	42–43	283	2.9–3.0	0.6–1.2
D17	120.7004	23.7698	C	005–015	2.5	1.8	3.1	56–57	255	1.6–1.7	0.6–0.9
D18	120.7004	23.7697	C	005–015	1.1	2.2	2.5	29–30	255	1.9–2.0	0.7–1.1
D19	120.6947	23.7486	C	020–030	2.5	1.3–1.5	2.8–2.9	61–67	257–265	0.9–1.4	0.7–0.9
E1	120.6540	23.6578	C	025–035	0.8	1.9–2.0	2.1–2.2	58–90	205–229	0.0–0.5	1.8–2.0
E2	120.6535	23.6574	C	060–070	0.2	0.9–1.0	0.9–1.0	22–90	240–280	0.0–0.5	0.7–1.0
E3	120.6524	23.6562	C	025–035	0.4	2.2	2.2	45–90	215	0.0–0.06	2.3–2.4
E4	120.6507	23.6543	D	041–051	0.5	2.36	2.41	68–90	240	0.05	2.36
E5	120.6486	23.6517	C	050–060	0.4	2.0	2.0	39–90	230–254	0.0–0.5	1.9–2.0
E6	120.6481	23.6515	C	055–065	0.4	1.1–1.2	1.1–1.3	39–90	235–268	0.0–0.5	1.0–1.1

[a] A1–A8: Taan River valley; A9–A24: Tachia River valley; B1–B21: Tachia River valley-Wufeng; C1–C27: Wufeng-Nantou; D1–D19: around Choushui River valley; E1–E6: around Tungtou.
[b] Positive: right-lateral slip; negative: left lateral slip.

but not its frontal part, had moved (to the north) opposite to its initial motion (to the southwest-west), the net slip values of this thrust block (by GPS) may be smaller than those surveyed on the surface rupture.

5.2. Discrepancy with seismological data

Although diverging, the fault dip-angles we obtained (mostly $>30°$; Fig. 7d) are apparently larger than the dip-angle of the seismogenic fault (20–30°) based on earthquake fault plane solutions (Kao and Chen, 2000). The surface rupture was commonly associated with a broad anticlinal fold on the hanging-wall side. The entire shortening across the rupture thus could be underestimated at many sites. This would yield an apparent, larger fault-dip angle (e.g. Fig. 3). On the other hand, we observed that the fault plane of the rupture was commonly parallel to the bedding of the bedrock, where exposed adjacent to the rupture. Note that near the rupture the strata generally dip at $>40°$, which are comparable with most of the fault-dip angles we calculated. We thus argue that the error of our obtained fault dip-angle is minor and cannot account for the total difference in dip-angle between the surface and seimogenic faults. Instead, we believe that the seimogenic fault steepens as it propagated to the surface.

Perhaps the greatest inconsistency between the surface rupture measurements and the seismological data occurs where the rupture ends to the north and to the south. Apparently, there is no surface rupture related to the final subevent of the main shock determined by Kao and Chen (2000). In addition, the strike-slip fault zones defined by the aftershock sequences (Kao and Chen, 2000), which may serve as lateral ramps of the thrust block in depth, are unclear on the surface. In the Tachia and Taan river valleys in the north, our data suggest that the regionally NNW-directed thrusting by GPS was partitioned into two parts,

one N-directed and another NW-directed; both are characterized by pure thrusting along distinct segments of the rupture (Figs. 4 and 9). In the south, the seismogenic NW-trending left-lateral fault may link to the deformations along the Luliao fault. However, these deformations are recognized for only several kilometers in length, much shorter than the seismogenic fault that extends for 50 km (Kao and Chen, 2000). The surface rupture in fact bends southwestward before it ends. The dominant right-lateral slip there does not appear to correspond to any right-lateral focal mechanisms from subevents of the main shock or aftershocks.

The lack of the surface expression of the seismogenic faults to the north and to the south suggests that the movement of these faults in the deeper crust is accommodated by wide deformational zones as they propagate to the surface. On the other hand, both the ending parts of the surface rupture may initiate at a relatively shallow crust. They may be triggered by the major seismogenic burst and move 'passively' during the earthquake. The characteristics of these portions of the surface rupture thus could reflect the strain condition of the crust shallower than the seismogenic zone. Still, how and why the strain in the shallow crust accumulated before the earthquake remains unclear.

Acknowledgements

This study is sponsored by the Central Geological Survey, ROC and National Science Council, Taiwan, ROC. We greatly thank Dr Hui-Cheng Chang of the Geological Survey for his kindly support and helpful discussion. We also thank Dr Tom Fumal and Dr James Evans of Utah State University for their kindly review of this paper. Gratitude is also due to Mr Richard Heermance of Utah State University and Miss Hui-chi Kuo of National Taiwan Normal University for proof reading the manuscript of this paper.

Appendix A

See Table 1.

References

Central Geological Survey, 1999. Report of the Geological Survey of the 1999 Chi-Chi Earthquake. Central Geological Survey, Ministry of Economic Affairs, ROC (in Chinese).

Chang, S.L., 1971. Subsurface geologic study of the Taichung basin. Petroleum Geology of Taiwan 8, 21–45.

Chinese Petroleum Corporation, 1974. Geological map of Miaoli. Chinese Petroleum Corporation, ROC, scale 1:100,000.

Chinese Petroleum Corporation, 1982. Geological map of Taichung. Chinese Petroleum Corporation, ROC, scale 1:100,000.

Chinese Petroleum Corporation, 1986. Geological map of Chaiyi. Chinese Petroleum Corporation, ROC, scale 1:100,000.

Kao, H., Chen, W.P., 2000. The Chi-Chi earthquake sequence: active, out-of-sequence thrust faulting in Taiwan. Science 288, 2346–2439.

Ma, K.F., Mori, J., Lee, S.J., Yu, S.B., 2001. Spatial and temporal distribution of the slip for the 1999 Chi-Chi earthquake. Bulletin of Seismological Society of America 91 (5), 1068–1087.

Mori, J., Ma, K.F., 2000. Review of seismological results from the 1999 Chichi, Taiwan, earthquake. American Geophysical Union 2000 Fall Meeting Abstract, F873.

Sharp, R.V., 1975. Displacement on tectonic ruptures. California Division Mines and Geology Bulletin 196, 187–194.

Yu, S.B., Chen, H.Y., Kuo, L.C., 1997. Velocity field of GPS stations in the Taiwan area. Tectonophysics 274, 41–59.

Yu, S.B., Kuo, L.C., Hsu, Y.J., Su, H.H., Liu, C.C., 2001. Preseismic deformation and coseismic displacements associated with the 1999 Chi-Chi, Taiwan earthquake. Bulletin of Seismological Society of America 91 (5), 995–1012.